SECTION III - CHAPTER 6

6.1 Chapter introduction

This chapter deals with the fabrication and characterization of modified scaffolds; which were designed to improve the desirable properties and to minimize the drawbacks of SF and GG scaffolds. Main focus was to construct a better biomimmic scaffold with better swelling, degradation, drug delivery, mechanical and surface properties. A successful attempt was made to achieve this goal by fabricating the new scaffolds using silk fibroin and chitosan in different blend ratios. Moreover, the fabricated scaffolds were supplemented with two different antimicrobial agents *viz. cpr* and AgNPs, in order to get an initial strong antimicrobial effect followed by mild and prolonged antimicrobial properties latter on. The characterization was performed in two stages. In first stage, the detailed study and characterization was carried out to evaluate all the blend scaffolds and to select the best one on the basis of results. In second stage some more characterization studies were carried out only on selected scaffold.

6.2 Materials

Cocoons of *Bombex mori* silk worm were collected from local sericulture farm, Pilibhit, Uttar Pradesh, India. Chitosan with 85% degree of deacetylation, lysozyme (70,000 U/mg, EC 3.2.1.17, from hen egg white), lithium bromide (LiBr) and sodium bi carbonate ($NaHCO_3$) were procured from Sigma–Aldrich (USA). Ingredients of Nutrient Agar media (NA) Mueller Hinton Broth (MHB, complete media) media were sourced from Hi-Media Lab. Ltd. (Mumbai, India). AgNPs were synthesized in laboratory with aqueous extract of *Salvinia molesta* as described in chapter 4. The drug, *cpr*, was a kind gift from Elcon Drugs and formulations Ltd., Jaipur, India. All the chemicals utilized in this study were of analytical grade. All the aqueous solutions and media were prepared by using double distilled deionized water.

6.3 Methods

6.3.1 Preparation of polymeric solutions and scaffolds

Two polymeric solutions i.e. 2.0 % w/v chitosan (CS) and 2.0 % w/v silk fibroin (SF) were utilized in the study. CS solution was made by dissolving 2.0 % w/v chitosan in 2.0 % v/v glacial acetic acid under starring at 150 rpm up to 6h. The prepared CS solution was centrifuged at 1000 rpm for 5 min to remove the entrapped air bubbles. SF of 2.0 % w/v concentration was made by using the protocol described in 'Chapter 3, (3.2.1)'. Three different blends of SF and CS were prepared by blending SF and CS in three different (v/v) ratios of (2:1), (1:1) and (1:2). These blends were than supplemented with 1 mg/mL of *cpr* and 200 μg/mL of AgNPs. All the blends were than separately casted in to the glass moulds and then freezed at -50°C for 6h followed by lyophilization up to 48 h. The abbreviations S/C/NpCp (2:1), S/C/NpCp (1:1) and S/C/NpCp (1:2) have been assigned here to represent AgNPs and *cpr* containing SF-CS hybrid scaffolds of blend ratio (2:1), (1:1) and (1:2) respectively. Scaffolds of pure silk (SF_{sc}) and scaffold of pure chitosan (CS_{sc}) were also incorporated in the study as a control.

6.3.2 Post processing of fabricated scaffolds

After lyophilization all the scaffolds were immerged in 70% (v/v) ethanol for 30 min. Ethanol treatment induces insolubility to the silk component and neutralizes the acidity of chitosan [Jinkang et al., 2007]. Thereafter, all the scaffolds were immerged in PBS (pH 7.4) for 30 min followed by washing with deionized double distilled water. The post processed scaffolds were again lyophilized and subsequently used for the study.

6.3.3 Characterization of scaffolds and selection of best scaffold

All the scaffolds were primarily characterized before selecting the scaffold that is best suited for designing the wound dressing. Initially all the scaffolds were characterized though following studies and analytical techniques:

- Microstructure analysis through field emission scanning electron microscopy (FESEM, Zeiss Evo-18).
- Porosity measurement through liquid displacement method (Nazarov et. al., 2004).
- Evaluation of swelling characteristics in simulated wound fluid (SWF).
- Analysis of mechanical properties through universal testing machine (UTM, Instron 3369).
- Scaffold stability and degradability via in-vitro enzymatic degradation studies in SWF containing lysozyme (112U/mL)
- Drug (*cpr*) loading and release studies to evaluate *cpr* drug release behavior of scaffolds
- Studies on *cpr* release kinetics to predict the release mechanism
- FTIR analysis (FTIR spectrophotometer, Varian- 3100) for surface group analysis and to explore the interaction between polymers as well as between drug and polymers.
- XRD analysis (X-ray diffractometer, Rigaku Miniflex II) for exploring crystalinity and mutual interaction of polymers as well as drugs.

Detail procedures sample preparation and analysis are similar as discussed in Chapter 3; topic 3.2. After initial characterizations, properties of all the scaffolds were mutually compared on a five star grading scale and the best suited scaffold was chosen for further characterization and for designing the wound dressing.

6.3.4 Further characterization of selected scaffold

Following characterizations were performed after selecting the best suited scaffold for designing of wound dressing;

6.3.4.1 Confirmation of presence of AgNPs over the surface of scaffold

Presence of AgNPs on to the surface of scaffold was confirmed though high magnification FESEM imaging followed by surface elemental analysis though energy-dispersive X-ray (EDX) spectroscopy through associated EDX detector.

6.3.4.2 Release of silver from scaffold

Silver release studies were conducted in SWF at pH 6.0. A piece of scaffold was immerged in SWF with 1 mg/mL weight volume ratio. The system was than incubated at 37 °C. Samples (2 mL) were withdrawn at regular time interval of 24 h and same volume of fresh SWF was introduced in release medium to maintain the volume of release medium at constant. The amount of released silver in each sample solution was determined through atomic absorption spectrophotometer (AAS, Shimadzu AA-6300) using a hollow cathode lamp working at λ=328.1 nm. Before analysis of released silver, the calibration standard curve was plotted using AAS grade silver standard solution (Merk Millipore India Ltd., 1000 mg/L) of 1.0 ppm, 2.0 ppm, 3.0 ppm and 4.0 ppm concentrations. Double distilled deionized water with 0.5% nitric acid was used as blank. Standard curve used for determination of released silver has been given in *Fig 6.1*.

6.3.4.3 Verification of time dependent differential antimicrobial potential of selected scaffold

The antimicrobial property of selected scaffold was monitored by cell viability test at different times in two separate experiments to explore the change in antimicrobial potential of selected scaffold with passage of time. The cell viability tests were performed in two set of experiments using the same protocol described

in topic 3.2.13 of 'Chapter 3'. The first set of the cell viability studies were carried out by native scaffold whereas the second set of cell viability experiments were carried out by using the scaffold which were prior incubated in SWF for 24 h. The logic behind to do so is to know that, whether the scaffold remains antimicrobial effective or not after 24h, when no more *cpr* is releasing from the scaffold. Theoretically it is clear that in the first set of experiments *cpr* will act as primary antimicrobial agent due to initial fast release whereas in second set of study the AgNPs will mainly be responsible for the antimicrobial potential of scaffold.

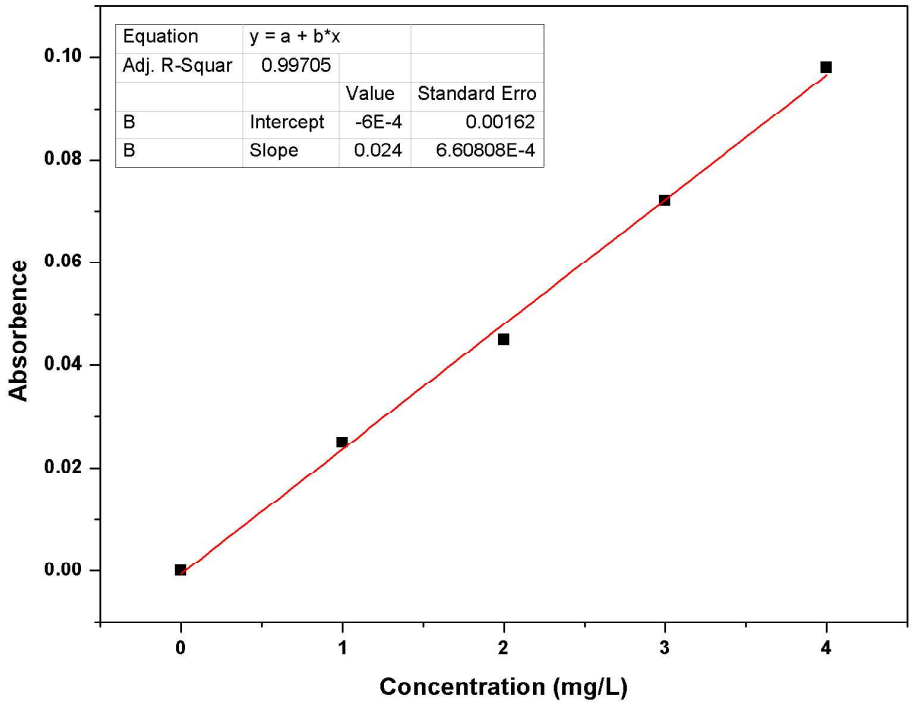

Fig 6.1 AAS standard curve for estimation of concentration of silver in the sample solution

6.3.4.4 Blood compatibility assay

The blood compatibility assay was performed according to standard procedure with minor amendments [Mehta et al., 2014]. The procedure of the assay, is similar as given in "Chapter 3 topic 3.3.11".

6.3.4.5 Water evaporation rate (WER)

WER for the selected scaffold was measured to evaluate the dehydration rate and moisture holding capacity of the blend scaffolds [Li et al., 2015]. The procedure of the assay, is similar as given in ‘‘Chapter 3 topic 3.3.11”.

6.3.4.6 Analysis of surface roughness by AFM

Surface topology and surface roughness of selected scaffold was analyzed through AFM (Dimension Edge, AFM-Bruker) using NT-MDT working in the contact mode. Screening areas was randomly selected over the sample and analyzed. AFM images have been processed using ‘NANOSCOPE’ software. Samples were prepared by cutting the scaffold in to thin small slice.

6.3.5 Designing of wound dressing

The wound dressing was designed by selected scaffold. A schematic diagram of the fabrication procedure has been presented in *Fig 6.2.*

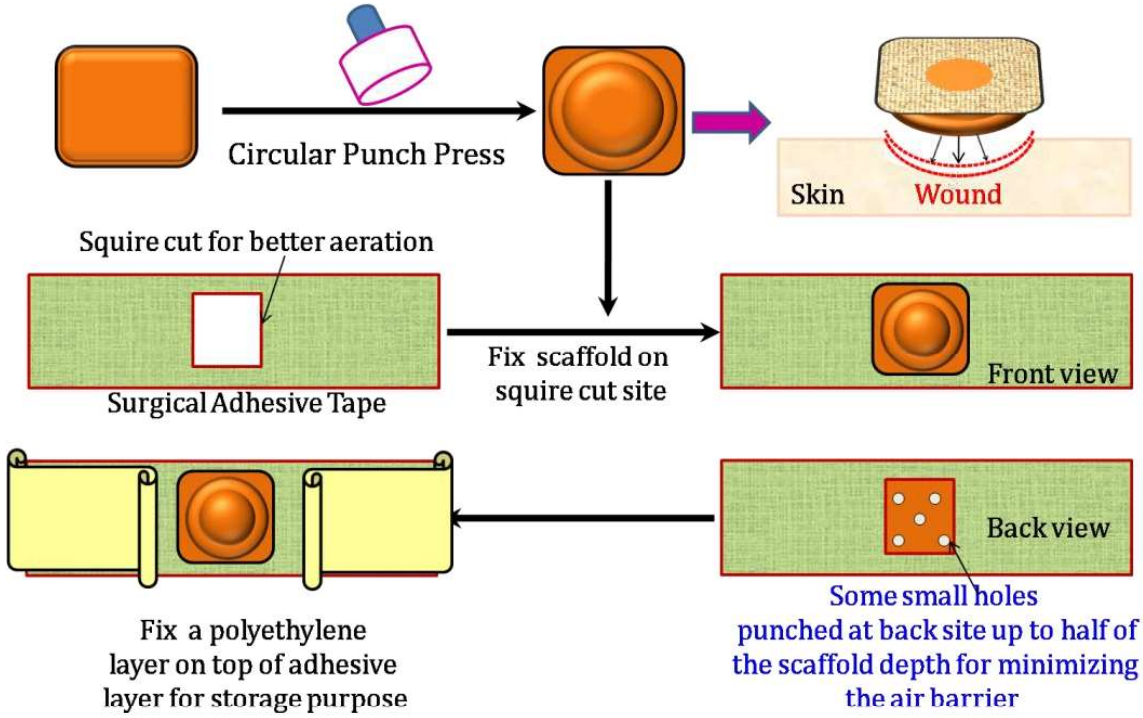

Fig 6.2 Schematic diagram showing methodology for designing of wound dressing

Briefly, in this study wound dressing was prepared to apply on a circular wound of 1.5 cm diameter. For dressing preparation; first of all the selected scaffold was cut into a squire piece of 2 cm×2 cm having thickness of 3 mm. After that the piece of scaffold was molded into a circular shape by pressing through a cylindrical glass tube (or circular punch press) of 1.5 cm diameter. Molded scaffold was then fixed over a squire cut of 1.5 cm edge on an adhesive surgical tape. Some small holes were than created on the backside of convex surface penetrated up to half of the dressing depth. The pores were created to further improve the gaseous exchange and to prevent the suboptimal level of oxygen supply at the healing site. Many perforated wound dressings are also available in the market with various trade names. It is being claimed by various commercialized wound dressing products (SilvaSorb™ of mediline, RGP 1083 Perforated™ of Raleigh Coatings Ltd. Scapa Soft-Pro™ of scapa healthcare) that perforation improves the quality of wound dressing through better exudate management and oxygen permeability. By keeping this fact in mind the wound dressing was made perforated up to half of the dressing depth. Full depth was not penetrated during perforation to maintain the scaffold native crosslink matrix at the contact site of wound. Finally a polyethylene protecting layer was fixed over the exposed adhesive surface of surgical tape.

6.3.6 In-vivo evaluation of designed wound dressing

6.3.6.1 Animals

Inbred Charles-Foster albino rats (150–170 g) of either sex were used as model animals for *invivo* wound healing experiments to evaluate the efficacy of designed wound dressing. Animals were obtained from central animal house of Institute of Medical Sciences, Banaras Hindu University, Varanasi, India. They were kept in the animal house at 26±7°C and relative humidity 44–56% under light and dark cycles of 10 and 14 h, respectively. The animals were fed with standard rodent

pellet diet and water. Food and water were given *ad libitum* throughout the experiments. Approval of 'Ethical Committee (IMS, BHU)' was taken before the experimental work (Annexure I). The guidelines as per "Principles of laboratory animal care" (NIH publication no. 82-23, revised 1985) were followed during whole period. Experiments were carried out in three groups in triplicate. Details of experimental groups are been given in *Table 6.1.*

Table 6.1 Experimental design of invivo study and details of experimental groups

Group information	Control Group (Cg)	Test groups (Tg)	
		Scaffold (dressing) without drug (S/C (1:1)) (Tg – 1)	Scaffold (dressing) with drug (S/C/NpCp (1:1)) (Tg – 2)
Group I	5	5	5
Group I	5	5	5
Group III	5	5	5
			Total animals needed =45

6.3.6.2 Surgical procedure

Rats were divided in to 3 groups with 15 animals in each group as enlisted in *Table 6.1*. Animals were anesthetized with diethyl ether and dorsal skin of rats was shaved and wiped with ethanol. An area of about 176 mm^2 (7.5 mm radius) was marked on the back of the rat by a standard ring. Full thickness of the marked skin was surgically removed. Wound of control group rats was left uncovered whereas wound of test groups were covered by dressing. Dressing without drug (S/C) and dressing with drug [S/C/NpCp (1:1)] was applied in two separate test groups. Wounds were traced on 1 mm graph paper on the day of wounding and subsequently at a gap period of 4 days until complete healing. Healing was

monitored by measuring the change in wound area regularly and the rate of wound contraction calculated as given in the formula below.

$$\%\, Wound\ contraction = \frac{S_0 - S_t}{S_0}$$

Where S_0 is initial wound area and S_t is wound area after time t. The animals were kept individually in separate cages to avoid scratching within the experimental group. The animals were killed using extra dose of anesthesia.

6.3.6.3 Histopathological examination

After the scarification of rat; the full thickness skin (25 mm^2) of from wound area was dissected for histopathological examination. The dissected samples were fixed in 10% buffered formalin. The fixed samples were washed and dehydrated before sectioning. Washing was done under running water for 2h. After washing; dehydration was carried out by transferring the samples into 30, 50, 70, 90 and 100% ethanol after subsequent interval of 1h. Dehydrated samples were treated with xyline for 15 min; xyline+wax for 40 min followed by wax_1, wax_2 and wax_3 for 30 min in each. Finally tissues were fixed in wax block for ease of sectioning. The fixed tissue was sectioned into 6µm sections using microtome (Leica Microsystems, USA). The tissue sections were fixed onto the gelatin coated glass slides and stained through hematoxylin-eocin reagents. First of all the tissues were stained with heamatoxylin for 5 min and then washed in running water for 15 min to remove the stain. After washing; the section was again dehydrated by upgraded concentrations of alcohol up to 70% and then dipped in eocin for 40 sec. Subsequent to eocin staining the samples were again washed with 70%, 90% and absolute alcohol for 10 min in each. At last, the tissue were treated with xylin for 10 min and mounted on the slide using DPX. The slide was left for whole night and histology was observed by optical microscope (Olympus).

6.4 Results and discussion

6.4.1 Morphology and ultra-structure (FESEM analysis) of fabricated scaffolds

Three hybrid scaffolds of silk fibroin and chitosan blends, loaded with *cpr* and AgNPs [S/C/NpCp (2:1), S/C/NpCp (1:1) & S/C/NpCp (1:2)] were fabricated through freeze drying method as previously descripted. Scaffolds of pure silk fibroin (SF_{sc}) and pure chitosan (CS_{sc}) were taken as control. External morphology and ultra structure of all the scaffolds through optical imaging and FESEM imaging respectively, has been shown in *Fig. 6.3*. Physical appearance of all the scaffolds was like sponge. The colour of blended scaffolds was brownish whereas control scaffolds were white in colour. The brown colour of blend scaffolds was due to incorporated AgNPs. The ultra-structure of scaffolds showed the porous and interconnected three dimensional matrixes. Interestingly the pore architecture and cross linking pattern were found to depend on blend ratio of both the polymers. SF_{sc} showed smallest average pore size 100 nm whereas CS_{sc} showed larger pore size distribution with average pore size of 185 nm. Pores of CS_{sc} were more interconnected than that of SF_{sc}. All the blended scaffolds have shown the intermediate pore size distribution. The average pore size of S/C/NpCp (2:1), S/C/NpCp (1:1) and S/C/NpCp (1:2) were 106 nm, 132 nm and 172 nm respectively.

6.4.2 Porosity measurement

Percentage porosities of scaffolds were measured by liquid displacement method using hexane as a displacement liquid because it penetrates inside the scaffolds without causing much shrinkage and swelling. All the scaffolds showed porosity ranging between 78 to 93%. Control scaffolds showed maximum (92.50% for SF_{sc}) and minimum (78.2% for CS) porosities. Among scaffolds of blends; S/C/NpCp (1:2), S/C/NpCp (1:1) and S/C/NpCp (2:1) have showed porosities 88.5±2.3, 85.2±1.2 and 81.4±3.6% porosities respectively. This is clear from the

results that porosities decrease with increase the content of chitosan in the blend. Porosity gradually depletes with increased chitosan amount due to combined effect of polymetic content and mutual cross-linking of silk and chitosan.

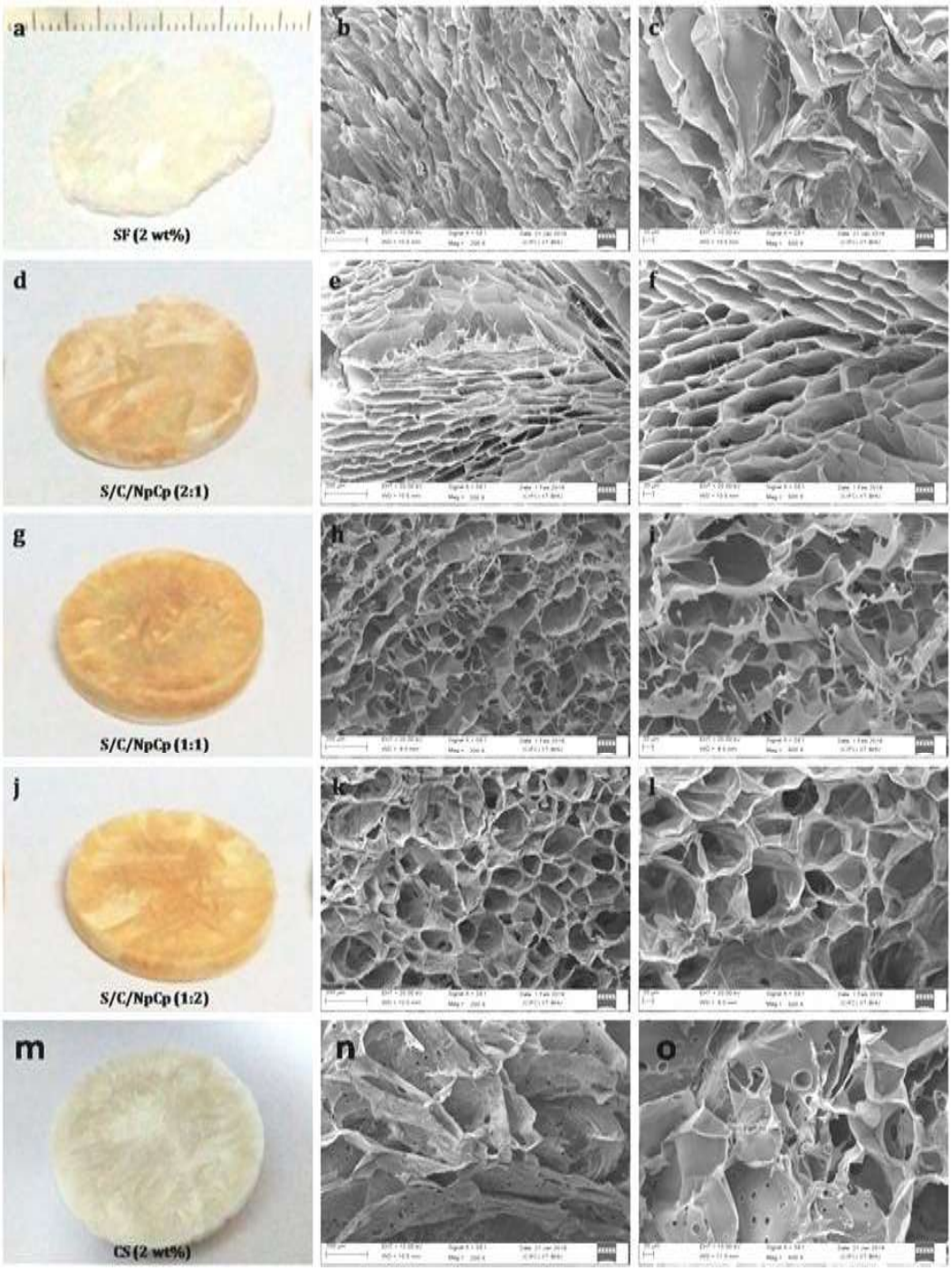

Fig 6.3 Optical images and FESEM images of all scaffolds (a-c) for SF_{sc} 2% w/v (d-f) for S/C/NpCp (2:1), (g-i) for S/C/NpCp (1:1), (j-l) for S/C/NpCp (1:2), (m-o) for CS_{sc} 2% w/v

6.4.3 Swelling Studies

Swelling study was carried out in order to evaluate the capacity of absorption of exudates by the scaffolds at wound site. These studies were conducted in SWF and obtained results are shown in Fig. *6.4.* On comparative basis it was found that SF_{sc} exhibited minimum whereas CS_{sc} showed maximum swelling properties in SWF. This difference in swelling behavior is due to their difference in native hydrophilicity. Chitosan is relatively more hydrophilic than silk fibroin thus shows better swelling ratio. In blend scaffolds; as the chitosan content increased the swelling ability also increases thus S/C/NpCp (2:1) showed better swelling than S/C/NpCp (1:2) while S/C/NpCp (1:1) has shown the intermediate swelling characteristics as expected.

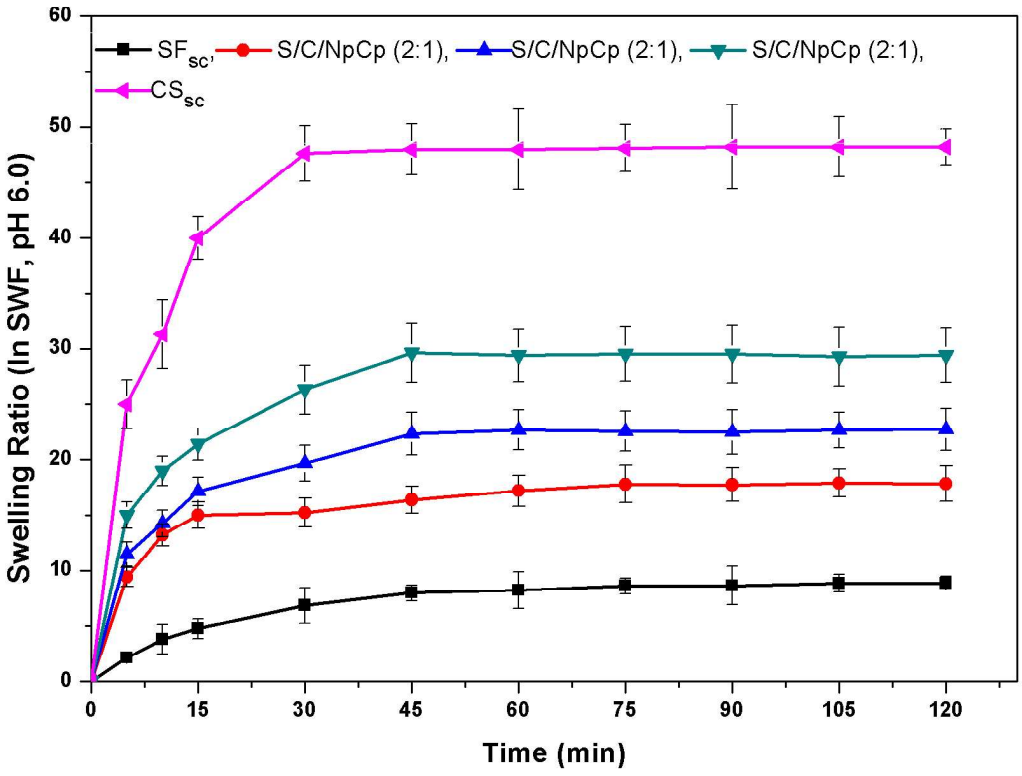

Fig. 6.4 Swelling behavior of SF_{sc}, CS_{sc}, S/C/NpCp (1:2), S/C/NpCp (1:1) and S/C/NpCp (2:1) scaffolds in SWF at pH 6.0

6.4.4 In-vitro enzymatic degradation studies

Degradability is an important desirable characteristic of biomaterials for some biomedical applications. For wound healing a moderate degradability rate is required so that on one hand the matrix of the scaffold could be able to provide the support for the proper cell growth and on the other hand it could subsequently be replaced from the native re-grown tissue. The matrix must not be degraded completely before proliferation phase and should not persist longer in remodeling phase i.e. after 4 months of post injury period. In the present study the degradability rates of scaffolds were evaluated through in-vitro degradation studies in SWF (pH 6.0) supplemented with 112 U/mL of lysozyme to better simulate the microenvironment of wound. Results of degradation study up to 28 days have been shown in *Fig 6.5*.

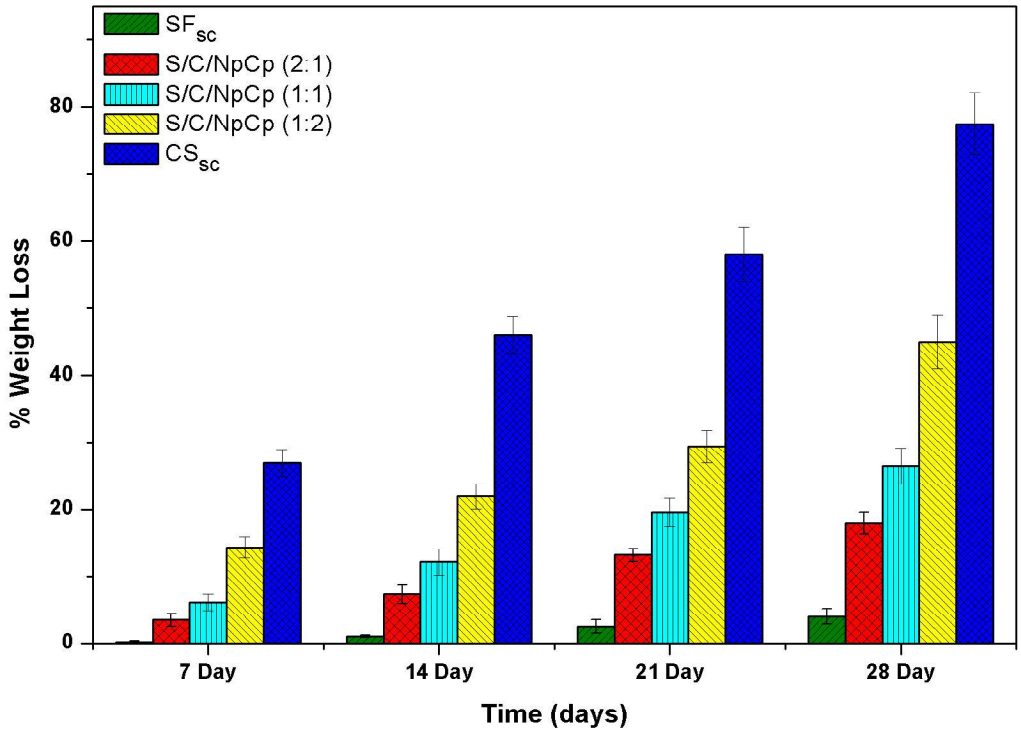

Fig. 6.5 Degradation behavior of SF_{sc}, CS_{sc}, S/C/NpCp (2:1), S/C/NpCp (1:1) and S/C/NpCp (1:2) scaffolds in SWF (pH 6.0, Temperature 37°C) containing lysozyme (112 U/mL)

The control SF_{sc} scaffolds showed very small degradation with only ~4.0% of reduction in weight in 28 days. This minor reduction in the weight of SF_{sc} could not be considered due to action of lysozyme because the lack of attacking site on the silk protein as descripted earlier in the 'Chapter 3'. CS_{sc} showed heighest degree of degradation with ~78.5% of weight loss in 28 days. The high degradation rate was due to lysozyme activity on chitosan. The addition of silk reduces the rate of degradation of chitosan. Blend scaffolds showed intermediate degradation rates variable with relative ratio of SF and CS. Therefore, it is clear from the results that the degradation rate can be tuned according to the need by adjusting the relative ratio of SF and CS in the blend solution. Scaffold, constructed through equal weight ratio of both polymers i.e. S/C/NpCp (1:1) was found to degrade by 27.2±2.2% in 28 days and takes 78 days to degrade completely.

6.4.5 Mechanical behavior of scaffolds

The mechanical behavior of scaffolds, expressed through stress strain curve, has been shown in *Fig 6.6*. All the samples were compressed up to 75% and their mechanical behavior was recorded as deformation pattern on applied load. *Fig 6.6* represents the ultimate compressive strengths at 75% compression (marked as * values) and compressive modulus (in inset) along with the stress strain curves. CS_{sc} scaffolds posses lest value of compressive strength and compressive modulus. Blending of both the polymers in equal ratio (S/C/NpCp (1:1)) has surprisingly increased both the compressive strength and compressive modulus of blend scaffold. This is due to the formation of compact structure through hydrogen bonding or ionic cross linking between silk and chitosan components of blend. Chan et al., has also found out that silk fibroin form β-sheet confirmation when blend with chitosan in some specific ratio [Chen et al., 1997]. Different researchers have claimed that both of these polymers interact together, either by hydrogen bonding

or through ionic interaction [Chen et al., 1997; Bhardwaj and Kundu, 2011]. Moreover, the increment in compressive strength and compressive modulus was maximum at 1:1 blend ratio whereas it was intermediate at 1:2 or 2:1 blend ratio. This behavior indicated that equal polymeric ratio is suitable for optimum cross linking while at unequal blend ratio; one of the polymer become limiting for the crosslinking.

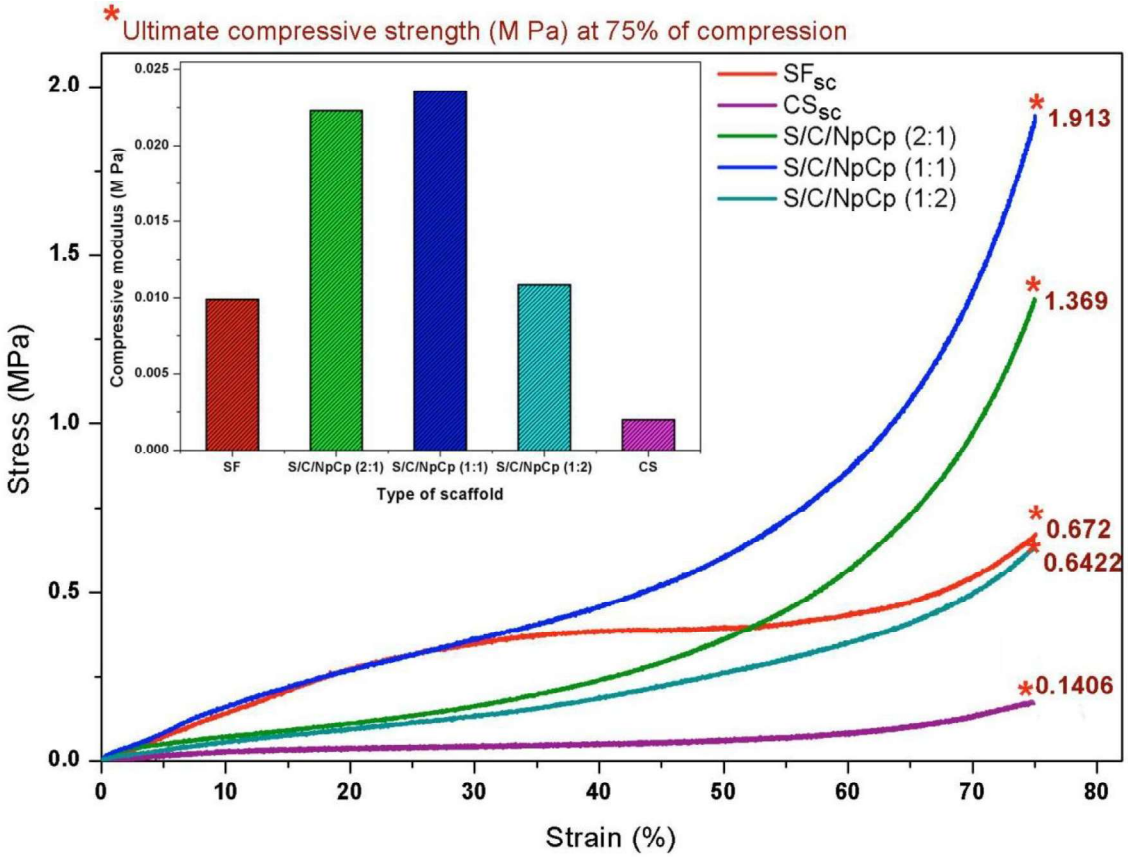

Fig 6.6 Ultimate compressive strengths at 75% compression (values marked as *) and compressive modulus (in inset) along with the stress strain curves of all scaffolds *viz.* SF_{sc}, CS_{sc}, S/C/NpCp (2:1), S/C/NpCp (1:1) and S/C/NpCp (1:2)

6.4.6 Drug loading and release studies

During evaluation of drug (*cpr*) loading efficiencies it was found that SF_{sc} scaffolds showed only 2.3±0.5% *cpr* loading affinity while CS_{sc} scaffolds showed to hold 3.2±0.4% of initial loaded drug. S/C/NpCp (2:1), S/C/NpCp (1:1) while S/C/NpCp (1:2) has shown *cpr* loading efficiencies 2.6±0.4, 2.9±0.6 and 3.0±0.5%

respectively. After loading studies the *cpr* release studies were carried out in SWF at pH 6.0 and the results are shown in *Fig. 6.7*. It is clear from the results that all the systems exhibited an initial strong bust release of *cpr*. Blending of silk fibroin with chitosan prolongs the release period of drug as compared to CS_{sc}. This is due to improved hydrophobicity of blend (in respect to CS_{sc}) thus decrease the rate of release of hydrophilic drug in aqueous medium of SWF.

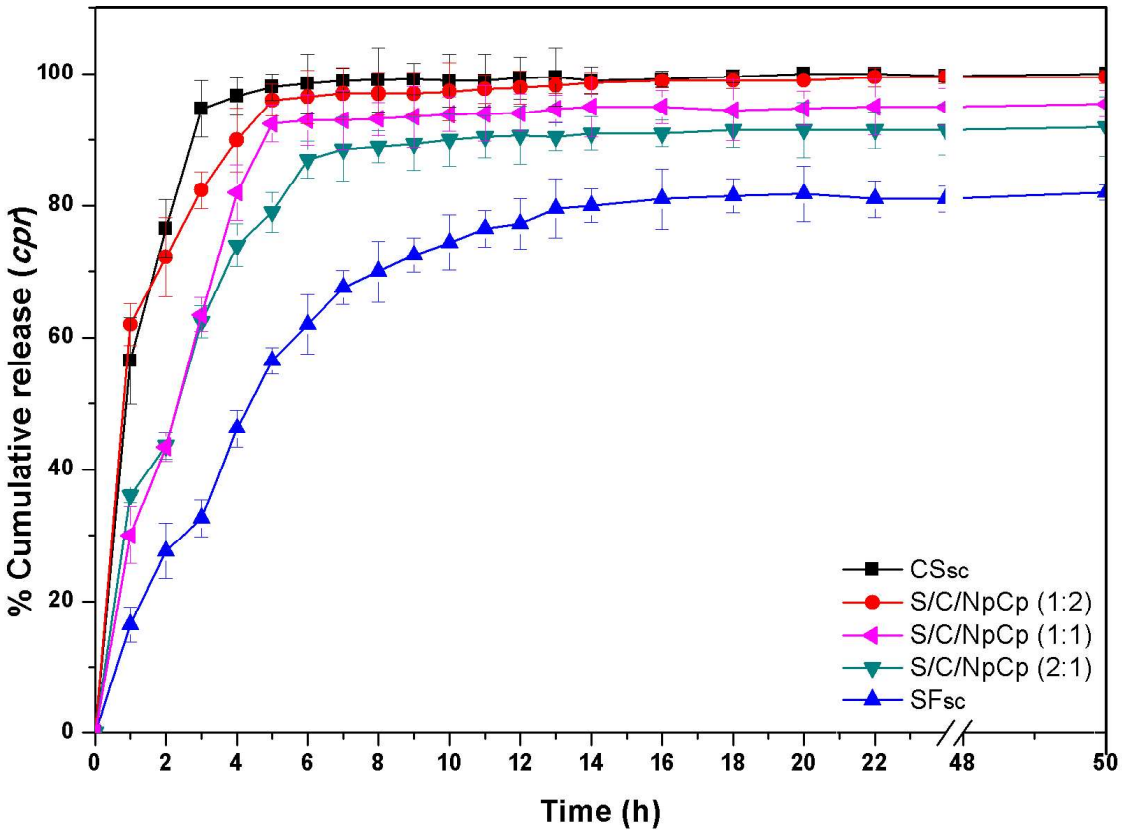

Fig. 6.7 Release pattern of *cpr* from SF_{sc}, CS_{sc}, S/C/NpCp (2:1), S/C/NpCp (1:1) and S/C/NpCp (1:2) in SWF at pH 6.0 and temperature 37°C

6.4.7 *cpr* release kinetics and release mechanism

The release data was fitted in to different in-vitro release kinetic models *viz.* zero order, first order, Higuchi and Korsmeyer-Peppas model to calculate kinetic parameters and to predict release mechanism of *cpr* from scaffolds. Calculated kinetic parameters have been enlisted in *Table 6.2*. It is clear from the results that

release of *cpr* from all the scaffolds followed the Korsmeyer-Peppas kinetic model with regression coefficient (R^2) >0.9. The values of release exponents (n) were; 0.45<n<0.89 for all the systems which indicated that *cpr* mainly released through anomalous (non-Fickian) diffusion and the whole release process is together governed by swelling, gel formation, diffusion and degradation of polymeric matrix [Costa and Lobo, 2001; Singhvi and Singh, 2011]. Moreover, regression coefficients are also in good agreement with Higuchi kinetic model which indicated that some portion of drug also release through Fickian diffusion [Desai et al., 1966].

Table 6.2 Kinetic parameters of cpr release from different scaffolds

Kinetic Model	Parameter	System				
		SF_{sc}	S/C/NpCp (2:1)	S/C/NpCp (1:1)	S/C/NpCp (1:2)	CS_{sc}
Zero order	k	20.31	25.36	28.26	32.78	32.92
	R^2	0.835	0.688	0.636	0.459	0.407
First order	k	0.067	0.116	0.097	0.088	0.078
	R^2	0.908	0.815	0.811	0.700	0.838
Higuchi	k	43.30	48.11	49.50	52.82	53.24
	R^2	0.970	0.966	0.958	0.903	0.944
Korsmeyer-Peppas	n	0.458	0.557	0.468	0.454	0.456
	k	0.990	46.84	53.75	63.16	71.25
	R^2	0.983	0.970	0.967	0.916	0.978

6.4.8 FTIR analysis

Fig. 6.8 represents the IR spectra (2500-400 cm^{-1}) of all blend and control scaffolds along with IR spectra of *cpr* and AgNPs for compare. All IR spectra showed multiple bands. Details of bands in controls (SF_{sc}, CS_{sc}, *cpr* and AgNPs) and their assignments have been enlisted in *Table 6.3*. In the IR spectra of blend scaffolds some siftings and some new bands appeared as compared with the IR spectra of controls. All the scaffolds of SF-CS blends has showed a common band around 1654 cm^{-1} which represent the interaction between Amide I of SF_{sc} (1640 cm^{-1}) and –C=O stretching of CS_{sc} (1649 cm^{-1}). These both groups probably interact together though intermolecular hydrogen bonding.

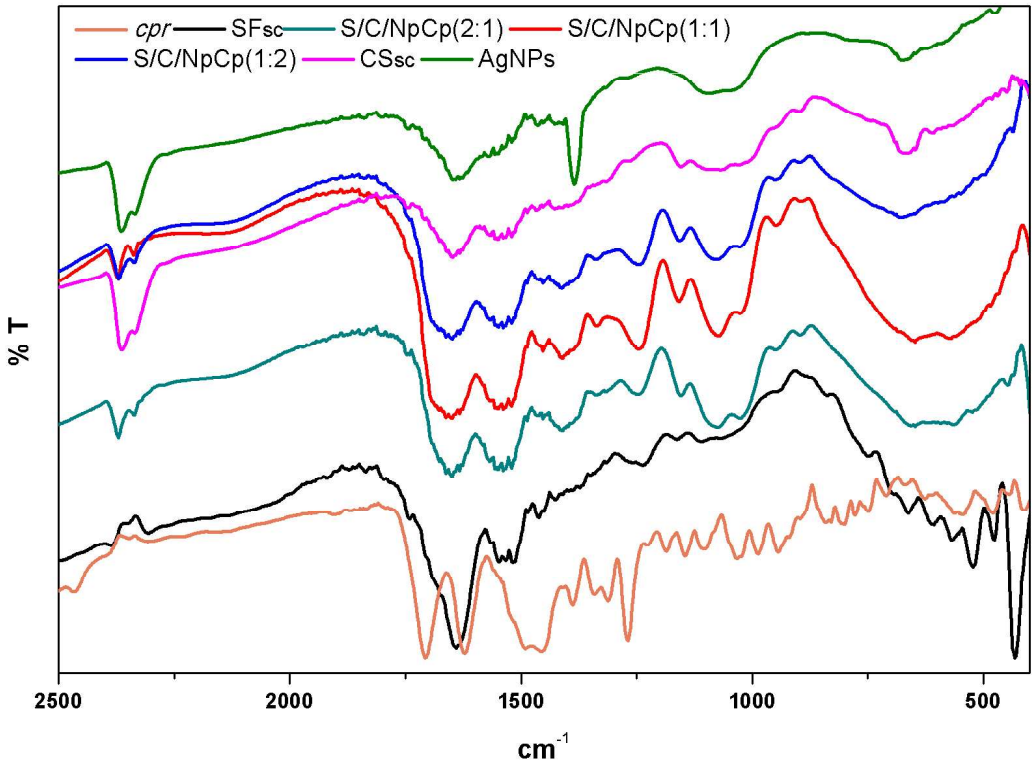

Fig 6.8 FTIR spectra of control and blend scaffolds viz. SF_{sc}, CS_{sc}, S/C/NpCp (2:1), S/C/NpCp (1:1) and S/C/NpCp (1:2) along with the FTIR spectra of drug *cpr* and AgNPs

This prediction of interaction between SF and CS is also supported by the results of mechanical behavior in this study where scaffolds of blends have shown

superior mechanical properties due to mutual crosslinking. Similar behavior of silk-chitosan blends has also been reported by other researchers [Chen et al., 1997; Bhardwaj and Kundu , 2011]. Moreover two new distinct bands around 1413 cm^{-1} and 1074 cm^{-1} in all blend scaffolds may be due to presence of AgNPs and *cpr* in the polymeric matrix. A minor sift in the characteristic C-O-C stretching vibration band of saccharide skeleton of CS from 1157 cm^{-1} to 1161 cm^{-1} is also the repetitive of interaction between both the polymers.

Table 6.3 Characteristic bands and their assignments in controls viz. SF, CS, cpr, AgNPs

System	Band (cm^{-1})	Assignment	Reference
SF_{sc}	1640	Amide I, C=O *s*, CN *s*, Random coil	Moraes et al, 2010
	1541	Amide II, NH *ib*, α-Halix	Ling et al, 2013
	1530	Amide II, NH *ib*, C-N *s*, β sheet	Ling et al, 2013
	1233	Amide III, N-H *s*, C-N *s*	Sionkowska et al, 2013
	1166	C-O-C sν,	Sionkowska et al, 2013
CS_{sc}	1649	C=O s,	Chan et al., 1997
	1543	NH_2 *b*	Chan et al., 1997
	1456	CH_2 b, CO_3^{--}, Pyrrolidine ring	Ling et al, 2013 Sionkowska et al, 2013
	1157	C-O-C *sν* of saccharide skeleton	Moraes et al, 2010, Sionkowska et al, 2013
	1032	C-O-C *s*	Chan et al., 1997
	898	Saccharide structure,	Moraes et al, 2010
Cpr	1705	C=O *sν*, carbonyl group of acid	Sahoo et al., 2012
	1623	δN-H *b* of quinolines	Sahoo et al., 2012
	1460	-C-O- *sν*	Sahoo et al., 2012
	1274	δO-H *b*	Sahoo et al., 2012
	1040	C-F *s*	Sahoo et al., 2012
AgNPs	1639	CN *s* of Amide I	Moraes et al, 2010
	1381	C=O *s* of –COOH	Verma et al., 2016

Abbreviations: ***s***: stretching; ***sν:*** stretching vibration; ***b:*** bending ; ***ib***: in-plane bending.

6.4.9 XRD analysis

To confirm the conformational changes, X-ray diffraction curves of all blend and control scaffolds were examined (*Fig. 6.9*). X-ray diffraction pattern of *cpr* and AgNPs have also been incorporated for compare. CS_{sc} scaffold showed the broad peaks at 2θ of 9.3° and 19.7° which corresponding to the crystalline structure of anhydrous chitosan and are assigned to crystal forms I and II [Ma et al., 2008, Bhardwaj and Kundu, 2011, Fan et al., 2009]. Pure SF scaffold showed a broad peak at 2θ=20.2° which corresponding to the β sheet crystalline structure of silk II [Asakura et al., 1985]. Scaffolds of blends with higher proportion of silk i.e. S/C/NpCp (2:1), showed broader band around 2θ=20° while S/C/NpCp (1:2) in which chitosan is in higher proportion showed comparatively sharper peak at 2θ=20.9°.

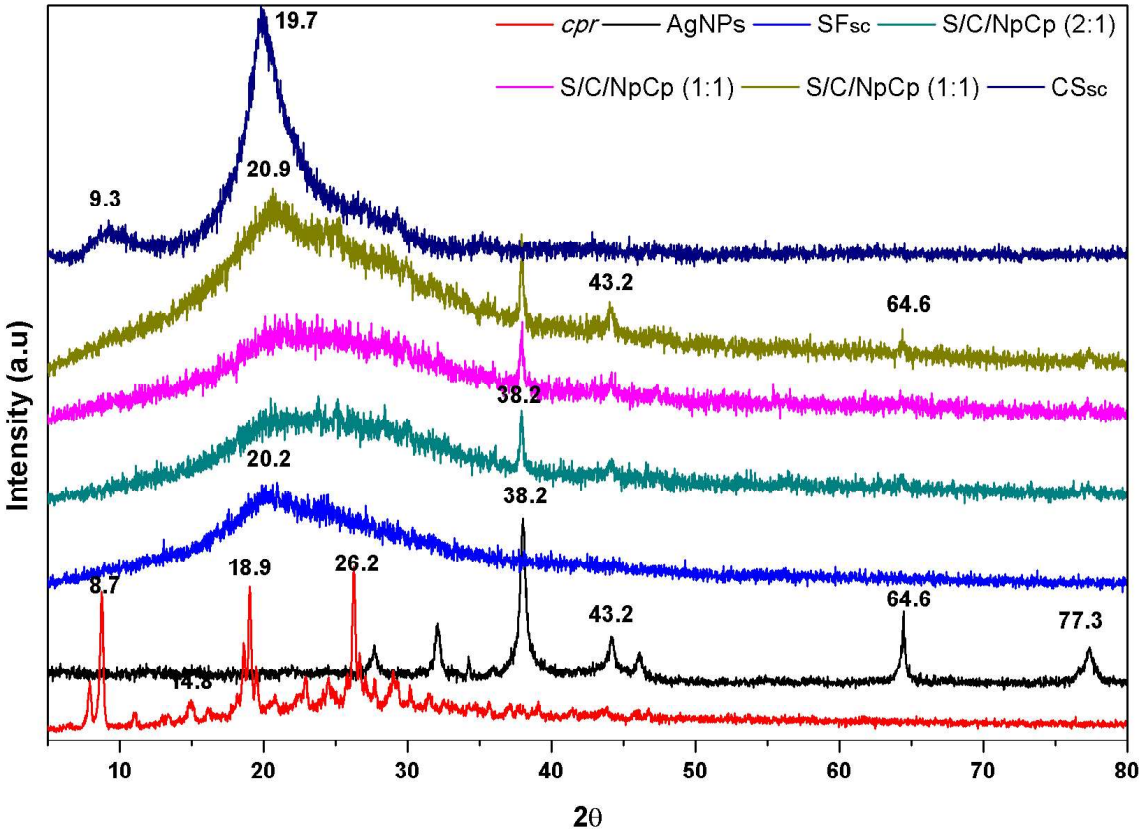

Fig. 6.9 X-ray diffraction patterns of SF_{sc}, CS_{sc}, S/C/NpCp (2:1), S/C/NpCp (1:1) and S/C/NpCp (1:2), *cpr* and AgNPs

These patterns defines that crystallinity of blends varies with relative ratio of both the polymers. XRD pattern of S/C/NpCp (2:1), S/C/NpCp (1:1) and S/C/NpCp (1:2) also showed weak peaks at 2θ=38.2°, 43.2° and 64.6° which correspond to diffraction patterns of crystalline planes of AgNPs present in blend scaffolds. Characteristic peaks of AgNPs are weak because due to entrapment in polymeric matrix the crystalline planes of AgNPs are not much exposed for diffraction of incident X-rays. The drug *cpr* showed many diffraction peaks in its XRD pattern due to its crystalline nature but S/C/NpCp (2:1), S/C/NpCp (1:1) and S/C/NpCp (1:2) has not shown any characteristic diffraction peak of *cpr*. The absence of any diffraction peak of crystalline *cpr* in the XRD pattern of blend scaffolds indicated that *cpr* molecules were homogeneously distributed in the polymer matrix without forming any crystalline aggregates. Similar findings has also been obtained by *Demirci et al.,* in their study where they had not found any diffraction peak of ciprofloxacin when incorporated it in the polymeric matrix of poly(4-vinylbenzoic acid-co-(ar-vinylbenzyl) trimethylammonium chloride) (Demirci et al., 2014).

6.4.10 Selection of best scaffold for designing of wound dressing

Best scaffold was selected on the basis of their performances in above mentioned studies. The performances of all scaffolds were compared on five star grading scale as shown in *Table 6.4*. On the basis of relative characteristics S/C/NpCp (1:1) was chosen as the best scaffold for designing of wound dressing. Before making the wound dressing, some further characterization was also done for S/C/NpCp (1:1) to ensure its suitability for biomedical applications and dressing design. S/C/NpCp (1:1) was characterized for the presence of AgNPs over the surface of scaffold, silver release profile, haematocompatibiity, dehydration rate and surface roughness. After these characterizations and studies the S/C/NpCp (1:1) was used for designing the wound dressing.

Table 6.4 Comparison table; designed on five star grade scale for evaluation of the relative performances of scaffolds

Types of Scaffold	Properties					
	Porosity	Swelling Properties	Mechanical Strength	Drug release Properties	Degradation	Score
SF_{sc}	*****	*	****	*****	*	**16***
S/C/NpCp (2:1)	****	**	***	****	**	**15***
S/C/NpCp (1:1)	****	***	*****	***	***	**18***
S/C/NpCp (1:2)	****	****	**	***	****	**17***
CS_{sc}	***	*****	*	**	*****	**16***

(*)=Poor, (**)= Ok, (***)=Good, (****)=Very Good, (*****)=Excellent

6.4.11 Confirmation of presence of AgNPs over the surface of scaffold

Although the XRD spectra confirms the existence of AgNPs in the scaffold but to confirm the presence of AgNPs on the surface of scaffold matrix; the EDX analysis was performed along with FESEM imaging at high magnification (50 KX). The results are shown in *Fig 6.10.* FESEM imaging visually confirms the presence of AgNPs on to the surface of scaffold whereas the elemental analysis by EDX further confirms that granulated structures appearing in FESEM image are actually AgNPs. It is important to note here that the size of nanoparticles appearing in FESEM image is larger than 100 nm whereas the original average size of incorporated AgNPs was 12.46 nm. This ambiguity in appeared size is due to the coating of polymeric layer over the surface of nanoparticles during blending.

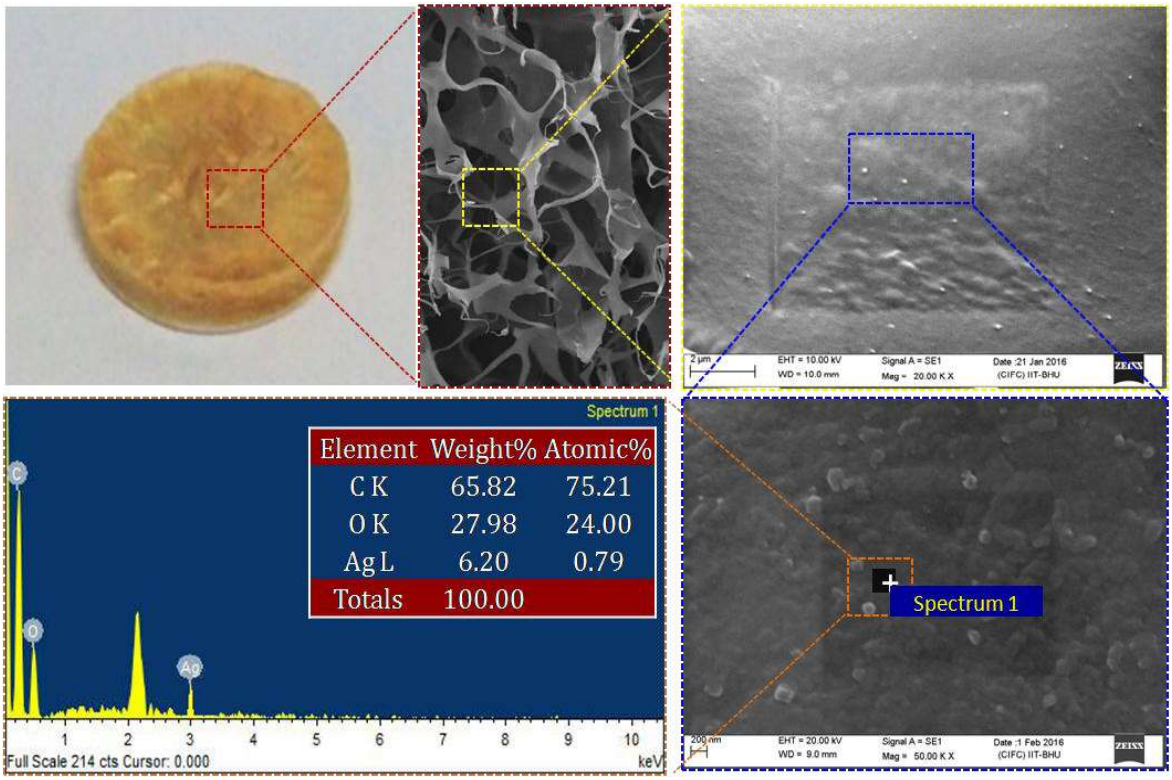

Fig 6.10 FESEM imaging of S/C/NpCp (1:1) scaffold with gradual increment in the magnification and associated EDX spectra for FESEM image at 50 KX magnification

6.4.12 Release of silver from S/C/NpCp (1:1)

After confirming the presence of AgNps on the surface of S/C/NpCp (1:1); the release of silver (as Ag^+ and intact AgNPs) in SWF at pH 6.0 was monitored up to 24 days through release studies. The released amount of silver in to release medium was analyzed by AAS. The obtained results are shown in *Fig. 6.11*. It was found that S/C/NpCp (1:1) was capable to release the silver in a controlled and sustained manner for a prolonged time. Unlike *cpr* release, the release of silver from S/C/NpCp (1:1) does not exhibit any initial burst release phase. This was due to slow release of Ag^+ and intact AgNPs from the scaffold.

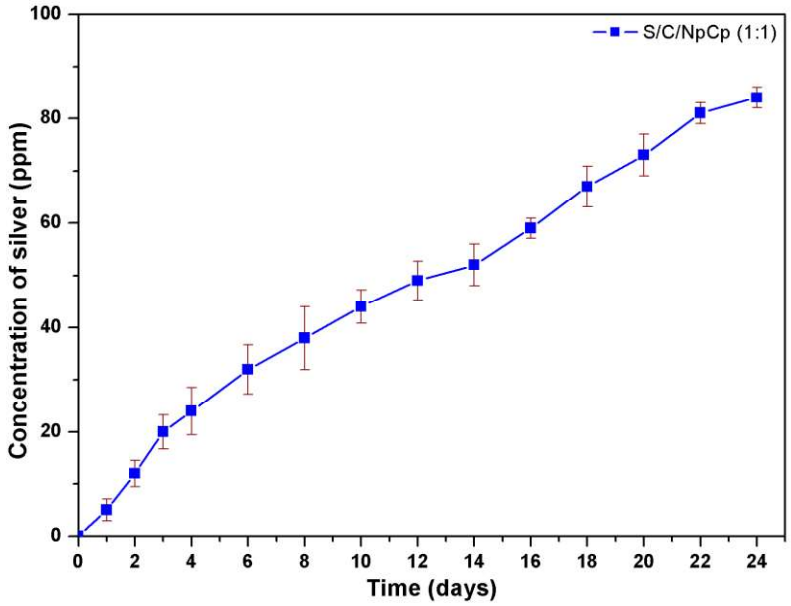

Fig 6.11 Release of silver from S/C/NpCp (1:1) in SWF at pH 6.0 and temperature 37°C

6.4.13 Evaluation of time dependent antimicrobial potential of S/C/NpCp (1:1)

The time dependent efficacy of S/C/NpCp (1:1) was evaluated though cell viability test against *E. coli* and *S. aureus*. It is clearly mentioned in methods section that these studies were carried out in two different set of experiments. First set of experiments were carried out with native S/C/NpCp (1:1) scaffold to evaluate initial antimicrobial potential of scaffold at the time of application whereas second set of experiments were conducted by the S/C/NpCp (1:1) scaffolds which were pre soaked in SWF for 24 h. Second set of experiments were targeted to evaluate the variation in the antimicrobial potential of S/C/NpCp (1:1) after 24h of application. The results for the first set of experiments are given in *Fig 6.12* while the results for the second set of experiments are given in *Fig 6.13.*

In the first set of experiments; the native S/C/NpCp (1:1) scaffold showed the strong antimicrobial activity with elimination of more than 98.0% of bacterial load within 4h. Whereas in second set of experiments, the S/C/NpCp (1:1) scaffold showed mild and decreased antimicrobial efficacy as compare with first set of

experiments. In the second set experiments, it was found that S/C/NpCp (1:1) takes 16h to remove more than 95.0 of initial bacterial load. This is because, in beginning the main strong antimicrobial effects comes from initial burst release of *cpr* from the scaffold while after 24 h release of *cpr* almost stops from scaffold (as evident from drug release studies) which lead to decreased antimicrobial potential. In the second set of experiments the main antimicrobial effect was provided by released silver rather than *cpr*. Moreover, it is also worth to note that chitosan itself has some antimicrobial properties thus its combined contribution during whole period of time should also be taken into consideration.

In the conclusion it can be said in the light of results of antimicrobial studies that S/C/NpCp (1:1) poses strong antimicrobial potential up to the period of continue release of *cpr* but once scaffold stops the release of *cpr* the antimicrobial potential of S/C/NpCp (1:1) becomes mild.

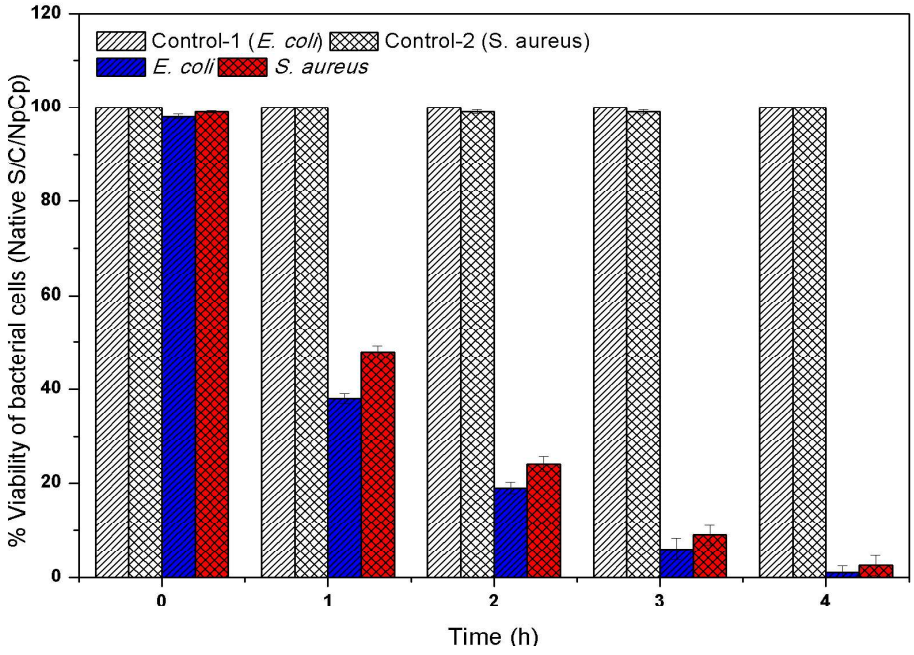

Fig 6.12 Cell viability test for first set of experiments which were conducted through native S/C/NpCp (1:1) scaffolds against *E. coli* and *S. aureus* in MHB

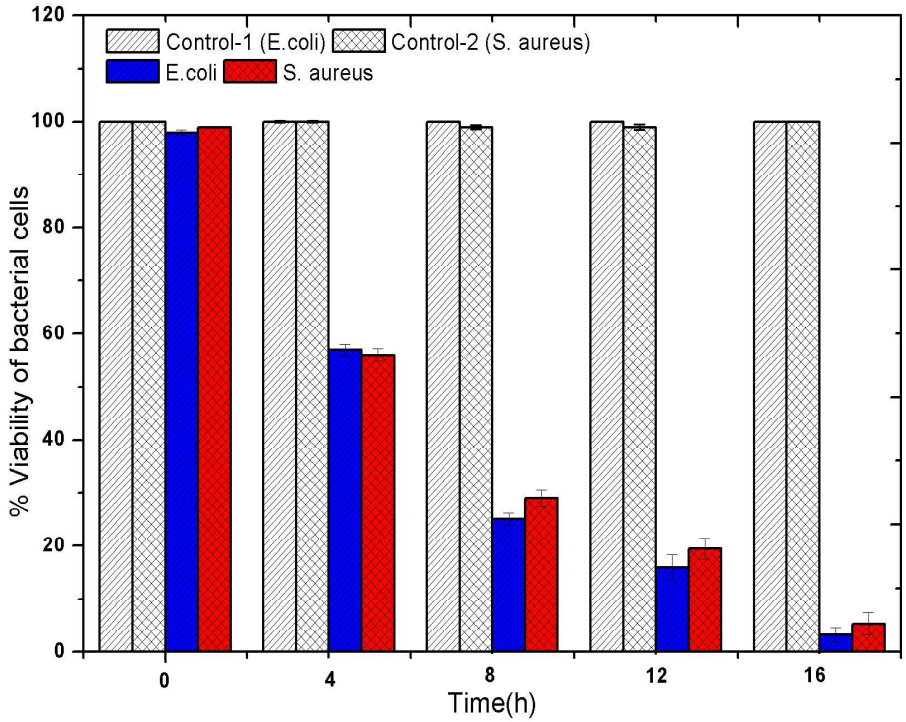

Fig 6.13 Cell viability test for the second set of cell viability experiments against *E. coli* and *S. aureus.* (*The experiments were conducted through S/C/NpCp (1:1) scaffolds which were pre soaked in SWF for 24 h before experiments. Soaking phase leads to removal of loaded cpr thus in second set of experiments mild antimicrobial effect comes from released silver from S/C/NpCp (1:1) in the form of* Ag^{+} *and intact AgNPs*)

6.4.14 Blood compatibility assay and dehydration test (WER)

Haemocompatibility or blood compatibility of S/C/NpCp (1:1) was determined by determining percentage hemolysis to test its suitability for being a wound dressing material. In the hemolysis test S/C/NpCp (1:1) had shown 2.9±0.6% hemolysis. Visual pattern of hemolysed blood is presented here as an optical image of the test in *Fig 6.14*. Because the percentage hemolysis is less than 5% hence the S/C/NpCp (1:1) scaffold can be considered highly haemocompatibe with human blood and can be used as a biomaterial for wound healing or tissue growth (Mehta et al., 2014, Abijeet et al., 2014).

Rate of dehydration was also evaluated through dehydration test and the dehydration profile was drawn as a function of remaining weight (%) vs time. The

obtained results have shown in *Fig. 6.15*. Swollen S/C/NpCp (1:1) exhibit slow dehydration rate and take 14 h to completely dehydrate at 37°C temperature and 35% relative humidity. The slow rate of dehydration is better for the material utilized to fabricate wound dressings and other biomaterials which are desired to provide moist environment at the site of application (Li et al., 2015). Herein, the developed scaffold (S/C/NpCp (1:1)) is suitable to provide moist environment at wound site.

Fig 6.14 Visual confirmation haemocompatibility of S/C/NpCp (1:1) by hemolytic activity shown by sample after incubation in physiological saline at 37°C for 1h

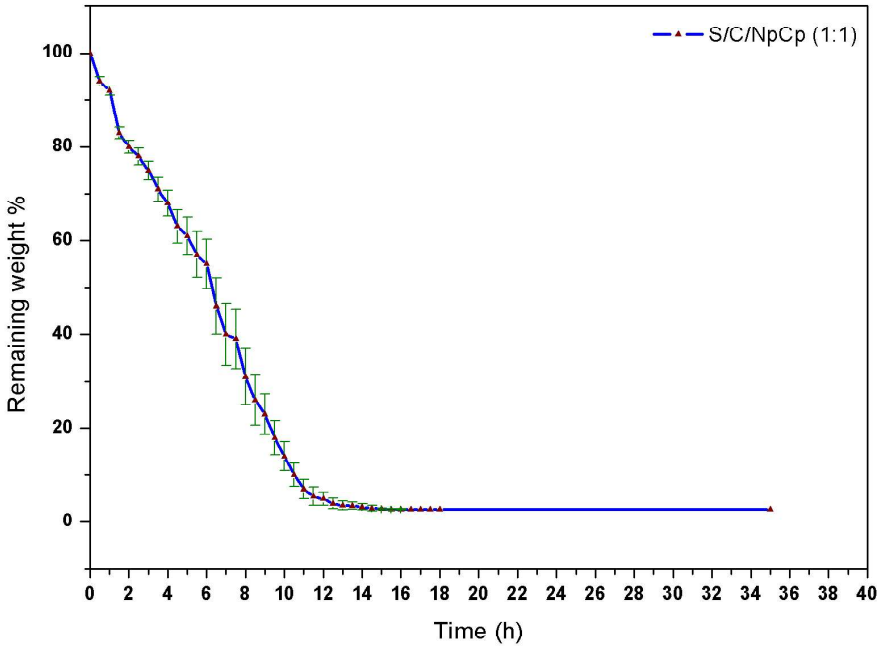

Fig. 6.15 Water loss from swollen S/C/NpCp (1:1) during dehydration 37°C temperature and 35% relative humidity

6.4.15 Surface topology and roughness (AFM analysis)

As descipted earlier in chapter 3, that the surface roughness is a crucial parameter for cell attachment, growth as well as migration thus rough surfaces are considered as better surfaces for tissue growth [Lampin et al., 1997, Anderson et al., 2006]. The AFM image of screened surface and its height index graph has been shown in *Fig 6.16 (a-c).* The values of mean absolute roughness (Ra), root mean squire roughness (Rq) and of maximum peak height (Rz) for S/C/NpCp (1:1) were found to be 163 nm, 222 nm and 866 nm respectively. These values are very close to native roughness parameters of extra cellular matrix [Anderson et al., 2006]. Therefore the surface of selected scaffold can be considered appropriate for the tissue growth and in-vivo applications.

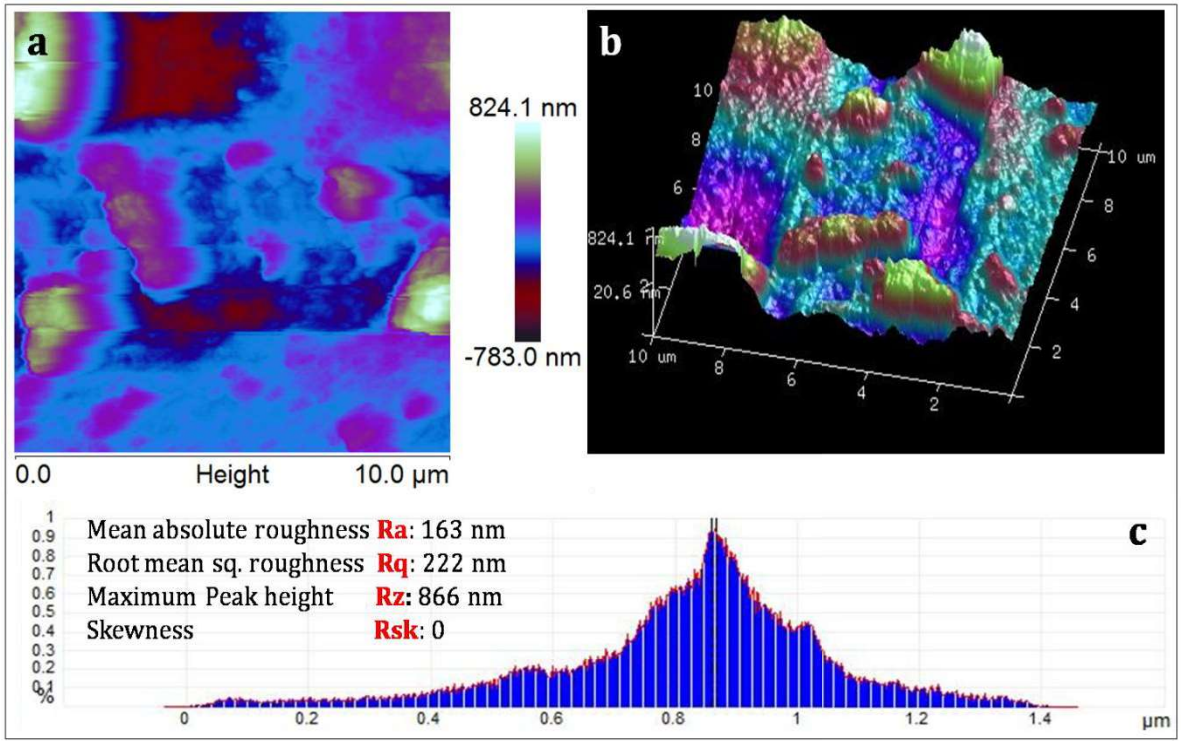

Fig 6.16 AFM image of randomly selected screened area on the S/C/NpCp (1:1); (a) 2D image of screened area (b) 3D image of screened area (c) height index curve of screened surface

6.4.16 Designing of the wound dressing

After selection and post selection characterization the wound dressing was designed according to the strategy described in material and method section; 6.3.5. After designing the wound dressing; it was evaluated for its wound healing potential through in-vivo studies.

6.4.17 Morphological examination of wound healing

Wound healing studies were carried out on Charles-Foster albino rats as model animals. The optical images of progressive wound healing in all groups are presented in *Fig 6.17.* Control group (Cg) was left untreated whereas the dressing was employed in two test groups; Test group 1(Tg-1) with dressing without drug S/C (1:1) and Test group 2(Tg-2) having dressing with drug i.e. S/C/NpCp (1:1). Each wound was observed on 4^{th}, 8^{th}, 12^{th}, 16^{th} and then daily up to complete healing. All rats survived throughout the post operative period until sacrificed.

At 4^{th} day after wounding; little discrete inflammation was observed in all groups. Minimum inflammation was observed in Tg-2 whereas inflammation was moderate in Cg. No visual wound contraction was observed in Cg while Tg-1 and Tg-2 showed very little visual contraction of wounds. Wounds of Cg had also shown the formation of scab. Some hemorrhagic tissue with yellow pus was also observable some wounds of Cg. One wound in Tg-1 also showed a minor infection whereas no infection was observed in any wound of Tg-2. Moreover, dressings were found to adhere on the wound surface and also absorbed the exudates from the wound surface. Although the outer surface of dressings was dry but inner surface i.e. the surface in the contact of wound was found moist therefore it can be said that dressing was capable of providing the moist environment at the wound vicinity.

After 8 days of wounding; the wounds of Cg were still scabbed but some visual contraction of wounds was observable. A little infection was still present in

some wounds of Cg. A very good degree of contraction in the wound size was observed in Tg-1 and Tg-2 groups. The maximum reduction in the size of wound was observed in animals of Tg-2 group.

At 12th day after wounding; all the wounds in Tg-2 were found almost healed whereas the wound area was still quite large in Cg. The animals of Tg-1 have also shown the great reduction in wound size with more than 90% closure of the wounded area. A little growth in the hairs was also seen in the healed area of Tg-1 and Tg-2. No significant growth in hairs was found in the wounded area of animals of Cg.

After 14 days of wounding; the wounds of Tg-1 were found to completely healed whereas wounds of animals of Tg-2 group had taken 18 days for complete healing. The wound in animals of Cg was found to completely heal in 21 days after wounding. So it is well clear from the observations that developed dressing is well effective in for the accelerated healing of wounds.

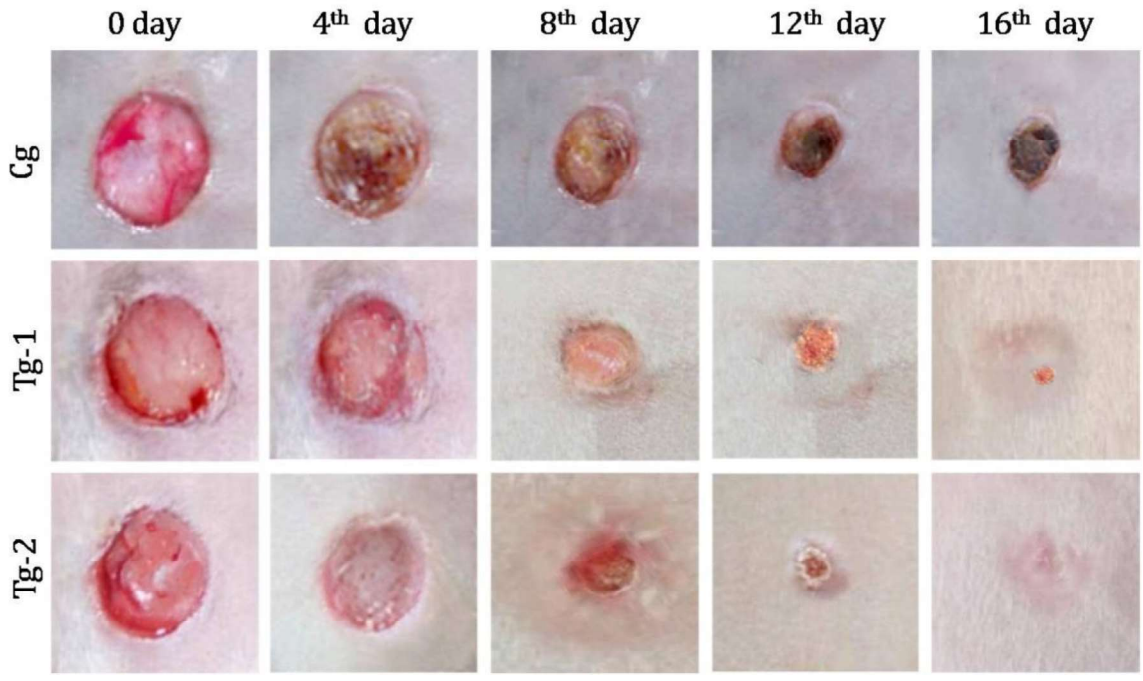

Fig 6.17 Optical images of open excision progressive wound healing in Charles-Foster albino rats for evaluating the wound healing efficiency of developed wound dressing by S/C/NpCp (1:1) scaffold

6.4.18 Statistical evaluation of wound healing

Statistical evaluation of wound healing was performed through monitoring consistent reduction in wound area with proceeding of time. The graphical pattern of wound size reduction is presented in *Fig 6.18*.

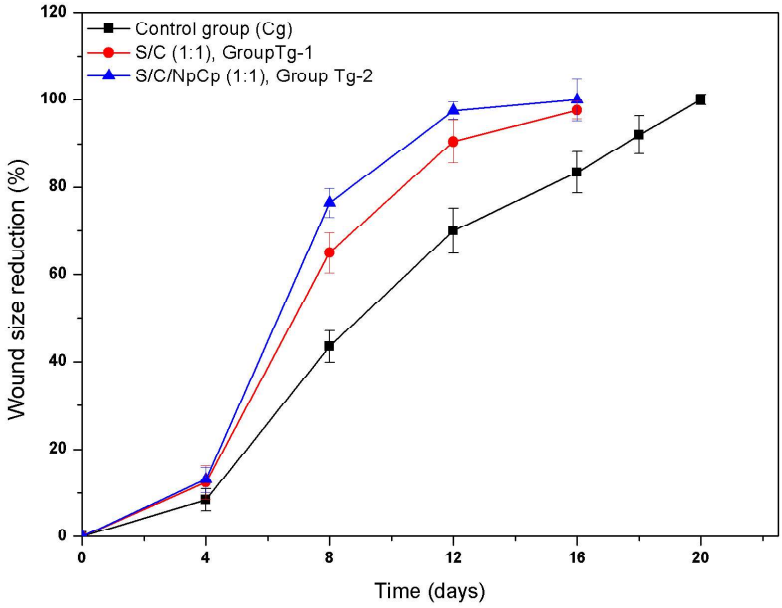

Fig 6.18 Percentage reduction in size of wound in the animals of different groups; Cg: control group, Tg-1: group treated with dressing without drug (S/C (1:1)) and Tg-2: group treated with dressing with drugs (S/C/NpCp (1:1))

It is clear from the results that wound closer rate was fastest in case of Tg-2 group in which the dressing with drug (S/C/NpCp (1:1)) was applied. The healing rate was slowest for control group (Cg) and was intermediate for group Tg-1, where the dressing without drug (S/C (1:1)) was applied. The results indicated that the developed wound dressing was highly effective for wound healing application and significantly reduce the healing time up to ~60%. The incorporation of *cpr* and AgNPs were also found to improve the healing capacity of developed wound dressing. Initial rate of wound size reduction was slow up to 4 days after wounding due to initial inflammatory phase. Maximum rate of healing was observed in the duration of day 4 to day 12. The wound was found to reduce by 97.5% in 12 days

when treated with drug loaded scaffold dressing (S/C/NpCp (1:1)) in Tg-2. In contrast to that the animals of control group has shown only 70% reduction in wound size in 12 days.

6.4.19 Histological studies

Histological examination of wounds was performed to depict the differential pattern of wound healing in different groups at histological level. Histological studies were performed though H&E staining of dissected tissue taken at 14th day after wounding. Day 14th was chosen for histological examination because of complete healing of wound in Tg-2 group. H&E staining of dissected tissue taken at the day of wounding (day 0) was also performed for comparative study. At day 0 only muscular layer is observable without any epidermis at wound site (*Fig 6.19, a*) due to removal of full thickness skin during creation of wound. Histology (at day 14th) of healed tissue in Cg, Tg-1 and Tg-2 has shown in *Fig 6.19, b, c & d* respectively. Normal skin appendages like hair follicles, blood capillaries and well arranged collagen fibers (white arrows) were not visible in control group. Epithelialization is not appeared to fully complete in control group-Cg in 14 days. Untreated wound of control group showed high number of inflammatory cells and granulated tissue as marked with back arrows. In group Tg-1 and Tg-2 the process of epithelialization is almost complete indicating the complete wound healing. But in group Tg-2 the histology of healed wound is more close to normal skin anatomy with well developed new hair follicles (Yellow arrows) and regenerated epithelial tissues as marked by blue arrows. Developing blood capillaries (white dashed arrows) are also visible in Tg-2 group. This indicates that *cpr* and AgNPs loaded S/C/NpCp (1:1) scaffold is more effective than the scaffold without drug i.e. S/C (1:1).

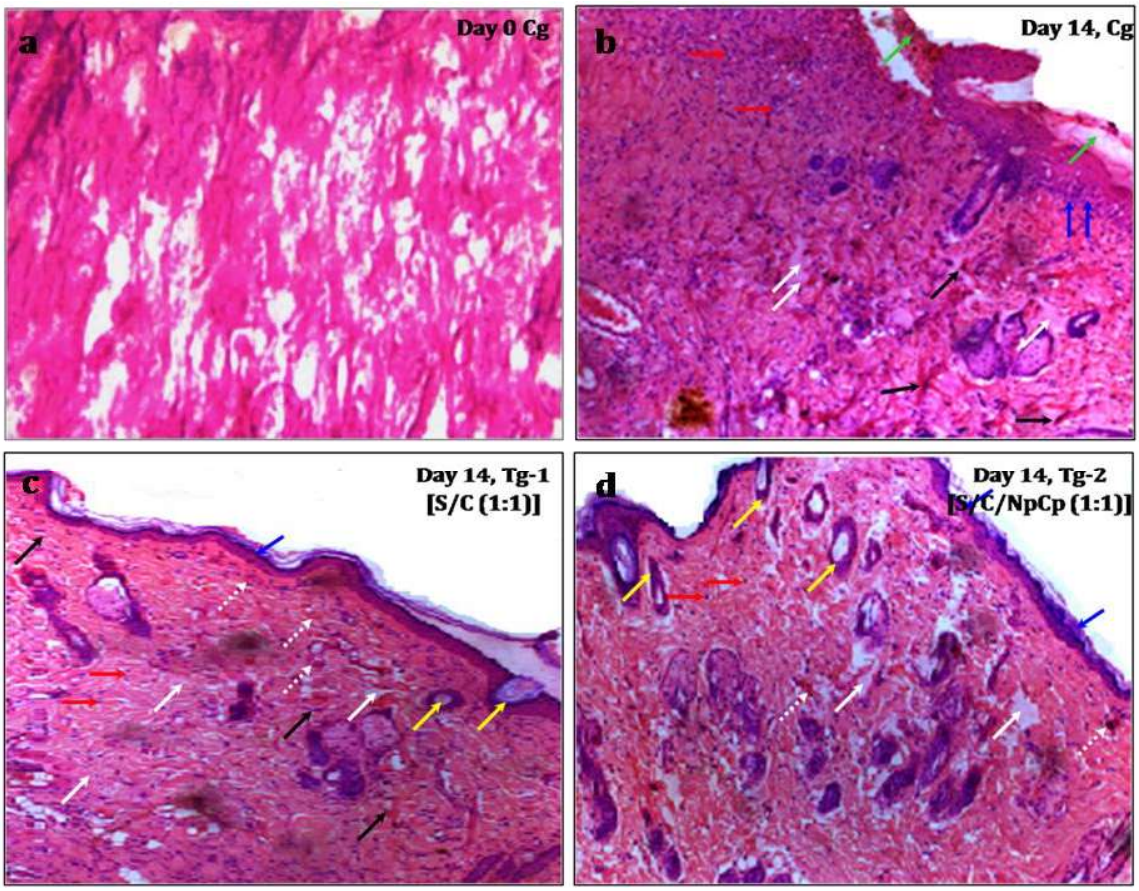

Fig 6.19 Histology of wound tissue (a) at day 0 in control group-Cg (b) at 14th post surgery day in Cg (c) at 14th post surgery day in group Tg-1 (d) at 14th post surgery day in group Tg-2. Blue arrows: *Re-grown epithelial tissue*; Green arrows: *Traumatic/ unhealed tissue*; Black arrows: *Fibroblast cells*; Red arrows: *Neutrophill cells*; White arrows: *Collagen fibbers*; Dashed white arrows: *Developing blood capillaries*; Yellow arrows: *Developing hair follicles*

6.5 Conclusion of chapter 6

Three different blends (v/v) ratios [(2:1), (1:1) and (1:2)] of SF and CS were utilized to fabricate the blend/hybrid scaffolds [S/C/NpCp (2:1), S/C/NpCp (1:1) and S/C/NpCp (1:2)] loaded with *cpr* and AgNPs. All the hybrid scaffolds along with the control scaffolds of pure silk (SF_{sc}) and pure chitosan (CS_{sc}) were studied for different physicochemical properties. FESEM showed that all the scaffolds were porous and percentage porosity was found to decreases with increase the amount of chitosan in blends. The average percentage porosities of S/C/NpCp (2:1), S/C/NpCp (1:1) and S/C/NpCp (1:2) were 88.5±2.3, 85.2±1.2 and 81.4±3.6% respectively.

Swelling ratio and degradation rate of the hybrid scaffolds can be tuned by varying the amount of chitosan in the blend. Swelling ratio increases with increasing CS content in hybrid scaffolds. SF_{sc} exhibited minimum (4.0%) and CS_{sc} showed maximum (78.5%) weight loss in 28 days whereas S/C/NpCp (1:1) degrades by 27.2±2.1% in 28 days. Mechanical properties showed an interesting behavior. Blending of both the polymers in equal ratio (S/C/NpCp (1:1)) has surprisingly increased both the compressive strength and compressive modulus of blend scaffold. This was due to the hydrogen bonding or ionic cross linking between SF and CS components of blend. XRD and FTIR analysis also supports this cross lining behavior of CS and SF. CS_{sc} showed strong *cpr* burst release rate during first 5h whereas SF_{sc} showed *cpr* release in a more sustained manner up to 14h by following Korsmeyer-Peppas kinetic model. After these studies, the results of all the scaffolds were mutually compared and on the basis of results; the S/C/NpCp (1:1) was selected for further characterization and for designing the wound dressing. S/C/NpCp (1:1) were found to be capable of releasing the silver in the form of Ag^{+} and intact AgNPs up to 24 days in a controlled and sustained manner. S/C/NpCp (1:1) was extremely hemocompatible and exhibited only 2.9±0.6% hemolysis. Mean absolute roughness (Ra) was 163 nm and the scaffold was found to take 14h for complete dehydration at 37°C and 35% relative humidity. Designed dressing was highly effective for wound healing purpose. Treated wounds healed only in 14 days whereas untreated wounds takes 21 days for complete healing.